CMS Physics Analysis Summary

Contact: cms-pag-conveners-exotica@cern.ch 2021/08/22

Search for heavy resonances and quantum black holes in eμ, eτ, and $\mu\tau$ final states in proton-proton collisions at $\sqrt{s} = 13$ TeV

The CMS Collaboration

Abstract

A search is reported for heavy resonances and quantum black holes decaying into eμ, eτ, and $\mu\tau$ final states in proton-proton collisions recorded by the CMS experiment at the CERN LHC at $\sqrt{s} = 13$ TeV, corresponding to an integrated luminosity of 137.1 fb^{-1}. No evidence is found for physics beyond the standard model in the dilepton invariant mass spectra, and upper limits are set at 95% confidence level on the products of the cross sections and branching fractions for various lepton-flavor violating signals. These include resonant τ sneutrino production in R-parity violating supersymmetric models, heavy Z' gauge bosons with lepton-flavor violating transitions, and non-resonant quantum black-hole production in models with extra spatial dimensions. In addition, model-independent limits are provided allowing the results to be interpreted in other models with the same final states and similar kinematic distributions. The results of these searches provide the best collider limits to date for the models considered.

1 Introduction

Several extensions of the standard model (SM) predict the existence of heavy particles that undergo lepton-flavor violating (LFV) decays, thereby motivating searches for deviations from the SM in $e\mu$, $e\tau$, and $\mu\tau$ final states. This note reports a search for such phenomena in the $e\mu$, $e\tau$ and $\mu\tau$ mass spectra. The analysis is based on data corresponding to an integrated luminosity of 137.1 fb^{-1} collected in proton-proton (pp) collisions at $\sqrt{s} = 13$ TeV in the CMS detector at the CERN LHC. The search strategy is designed to be model independent as much as possible. The results are interpreted in terms of the characteristics of the following predicted states: a τ sneutrino ($\widetilde{\nu}_\tau$), which can be the lightest supersymmetric particle (LSP) [1, 2] in R-parity violating (RPV) supersymmetric (SUSY) models [3], a heavy Z' gauge boson in LFV models [4], and quantum black holes (QBHs) [5, 6].

In RPV SUSY models, lepton flavor and lepton number are violated at Born level in interactions between fermions and their superpartners, where the $\widetilde{\nu}_\tau$ can be the LSP. For resonant $\widetilde{\nu}_\tau$ signals, the trilinear RPV part of the superpotential can be expressed as

$$W_{\mathrm{RPV}} = \frac{1}{2}\lambda_{ijk} L_i L_j \overline{E}_k + \lambda'_{ijk} L_i Q_j \overline{D}_k,$$

where i, j, and k are generation indices, L and Q are the $\mathrm{SU}(2)_L$ doublet superfields of the leptons and quarks, and $\overline{E}$ and $\overline{D}$ are the respective $\mathrm{SU}(2)_L$ singlet superfields of the charged leptons and down-like quarks. For simplicity, we assume that all RPV couplings vanish, except those that are connected to the production and decay of the $\widetilde{\nu}_\tau$, and we consider a SUSY mass hierarchy with $\widetilde{\nu}_\tau$ as the LSP. In this model, the $\widetilde{\nu}_\tau$ can be produced resonantly in pp collisions via the λ' coupling, and can decay either into dilepton final states via the λ couplings, or into quarks via the λ' coupling. We consider only the final states with two charged leptons. This analysis considers only $\widetilde{\nu}_\tau$ that decay promptly and not long-lived $\widetilde{\nu}_\tau$ [7], which could provide events with leptons from a displaced vertex.

An extension of the SM through the addition of an extra U(1) gauge symmetry provides a massive Z' vector boson [4]. In our search, we assume that the Z' boson has couplings similar to the Z boson in the SM, but that the Z' boson can also decay to the LFV $e\mu$, $e\tau$ and $\mu\tau$ final states with a branching fraction of 10% each.

Theories that invoke extra spatial dimensions can offer effective fundamental Planck scales in the TeV region. Such theories also provide the possibility of producing microscopic black holes [5, 6] at the LHC. In contrast to semiclassical thermal black holes that can decay to high-multiplicity final states, QBHs are nonthermal objects, expected to decay predominantly to pairs of particles. We consider the production of spin-0, colorless, neutral QBHs in a model with LFV [8], in which the cross section for QBH production depends on the threshold mass m_{th} in n additional spatial dimensions. The $n = 1$ possibility corresponds to the Randall–Sundrum (RS) brane-world model [9], and $n > 1$ corresponds to the Arkani–Hamed–Dimopoulos–Dvali (ADD) model [10]. While the resonant $\widetilde{\nu}_\tau$ and Z' signals generate narrow peaks in the invariant mass spectrum of the lepton pair, the distribution of the QBH signal is characterized by a sharp edge at the threshold of QBH production, followed by a monotonic decrease at larger masses.

Similar searches in LFV dilepton mass spectrum have been carried out by the CDF [11] and D0 [12] experiments at the Fermilab Tevatron in $\mathrm{p\overline{p}}$ collisions at a center-of-mass energy of 1.96 TeV and by the ATLAS and CMS experiments at the LHC in pp collisions at center-of-mass energies of 8 TeV [13, 14] and 13 TeV [15–17].

2 The CMS detector

The central feature of the CMS apparatus is a superconducting solenoid of 6 m internal diameter, providing a magnetic field of 3.8 T. Within the solenoid volume are a silicon pixel and strip tracker, a lead tungstate crystal electromagnetic calorimeter (ECAL), and a brass and scintillator hadron calorimeter (HCAL), each composed of a barrel and two endcap sections. Forward calorimeters extend the pseudorapidity coverage provided by the barrel and endcap detectors. Muons are detected in gas-ionization chambers embedded in the steel flux-return yoke outside the solenoid. Isolated particles of transverse momentum (p_T) of 100 GeV emitted at pseudorapidity range $|\eta| < 1.4$ have track resolutions of 2.8% in p_T and 10 (30) μm in the transverse (longitudinal) impact parameter [18]. The electron momentum is estimated by combining the energy measurement in the ECAL with the momentum measurement in the tracker. The momentum resolution for electrons with $p_T \approx 45$ GeV from $Z \to ee$ decays ranges from 1.7% to 4.5%. It is generally better in the barrel region than in the endcaps, and also depends on the bremsstrahlung energy emitted by the electron as it traverses the material in front of the ECAL [19]. Muons are measured in the pseudorapidity range $|\eta| < 2.4$, with detection planes made using three technologies: drift tubes, cathode strip chambers, and resistive plate chambers. The single muon trigger efficiency exceeds 90% over the full η range, and the efficiency to reconstruct and identify muons is greater than 96%. Matching muons to tracks measured in the silicon tracker results in a relative transverse momentum resolution, for muons with p_T up to 100 GeV, of 1% in the barrel and 3% in the endcaps. The p_T resolution in the barrel is better than 7% for muons with p_T up to 1 TeV [20]. A more detailed description of the CMS detector, together with a definition of the coordinate system used and the relevant kinematic variables, can be found in Ref. [21].

3 Collision data and simulated events

The data sample used for this analysis was collected during 2016, 2017, and 2018 pp collisions at a center-of-mass energy of 13 TeV. After applying data-quality requirements, the total integrated luminosity is 137.1 fb^{-1}.

Simulated samples of signal and background events are produced with several event generators. The RPV SUSY $\widetilde{\nu}_\tau$, Z', and QBH signal events are generated at leading order (LO) precision, using the CALCHEP 3.6 [22], PYTHIA 8.203 [23], and QBH 3.0 [8] Monte Carlo (MC) generators, respectively. The relative width of the Z' signal is taken as 3% of its mass. The RPV and QBH signals are generated with the CTEQ6L [24] parton distribution functions (PDF) while the Z' boson signals are simulated using the NNPDF 3.0 and 3.1 PDF sets [25]. The LO RPV SUSY $\widetilde{\nu}_\tau$ signal event yield is normalized to a next-to-leading order (NLO) calculation of the production cross section; in this calculation the factorization and renormalization scales are set to the mass of the $\widetilde{\nu}_\tau$.

The MADGRAPH5_aMC@NLO generator [26] is used for Z+jets production. They are simulated at NLO with the FxFx jet matching and merging [27]. Diboson production is simulated at LO using the PYTHIA generator. The POWHEG event generator [28–31] is used to simulate $t\bar{t}$ and single top processes. The cross sections used to normalize the contribution of these backgrounds are calculated at next-to-next-to-leading order for WW, ZZ, single top quark, and $t\bar{t}$ processes, and at NLO accuracy for WZ and Drell-Yan events. The POWHEG and MADGRAPH5_aMC@NLO generators are interfaced with PYTHIA for parton showering, fragmentation, and decays. The PYTHIA parameters for the underlying event description are set to the CUETP8M1 (CP5) tune [32] in 2016 (2017, 2018) simulated samples.

The generated events are processed through a full simulation of the CMS detector, based on GEANT4 [33–35]. The simulated events incorporate additional pp interactions within the same or a nearby bunch crossings, termed pileup, that are weighted to match the measured distribution of the number of interactions per bunch crossing in data. The simulated event samples are normalized to the integrated luminosity of the data. The products of the total acceptance and efficiency for the three signal models in this analysis are determined through MC simulation. The trigger and object reconstruction efficiencies are corrected to the values measured in data.

4 Event reconstruction and selection

The global event reconstruction is performed using a particle-flow (PF) algorithm [36], which reconstructs and identifies each individual particle with an optimized combination of all subdetector information. In this process, the identification of the particle type (photon, electron, muon, charged or neutral hadron) plays an important role in the determination of the particle direction and energy.

The candidate vertex with the largest value of summed physics-object p_{T}^2 is taken to be the primary pp interaction vertex. The physics objects are the jets, clustered using the jet finding algorithm [37, 38] with the tracks assigned to candidate vertices as inputs, and the associated missing transverse momentum, taken as the negative vector sum of the p_{T} of those jets.

To reconstruct an electron candidate, energy depositions in the ECAL are first combined into clusters, assuming that each cluster represents a single particle. The clusters are then combined in a way consistent with bremsstrahlung emission, to produce a single "supercluster", which represents the electron or photon. These superclusters are used to seed tracking algorithms, and if a resulting track is found, it is associated to the supercluster to form an electron candidate.

To reconstruct a muon candidate, hits are first fitted separately to trajectories in the inner tracker detector, and in the outer-muon system. The two trajectories are then combined in a global-muon track hypothesis.

Hadronic τ decays (τ_{h}) are reconstructed from jets, using the hadrons-plus-strips algorithm [39], which combines 1 or 3 tracks with energy deposits in the calorimeters, to identify the tau decay modes. Neutral pions are reconstructed as strips with dynamic size in η-ϕ from reconstructed electrons and photons, where the strip size varies as a function of the p_{T} of the electron or photon candidate.

To distinguish genuine τ_{h} decays from jets originating from the hadronization of quarks or gluons, and from electrons or muons, the DEEPTAU algorithm is used [40]. Information from all individual reconstructed particles near the τ_{h} axis is combined with properties of the τ_{h} candidate and the event. The rate of a jet to be misidentified as τ_{h} by the DEEPTAU algorithm depends on the p_{T} and quark flavor of the jet. In simulated events from W boson production in association with jets it has been estimated to be 0.43% for a genuine τ_{h} identification efficiency of 70%. The misidentification rate for electrons (muons) is 2.60 (0.03)% for a genuine τ_{h} identification efficiency of 80% (>99)%.

4.1 Selection in eμ final state

For the eμ selection, at least one prompt, isolated electron and at least one prompt, isolated muon in the event are required. This minimal selection facilitates a reinterpretation of the results in terms of models with more complex signal topologies than a single eμ pair.

Events that satisfy single-muon or single electromagnetic-cluster triggers with respective p_T thresholds of 50 and 175 GeV for muons and photons, respectively, are selected. In the year 2018, the p_T threshold of the photon trigger was raised to 200 GeV. Electromagnetic energy deposited by an electron in the calorimeter activates the photon trigger, and the photon trigger is therefore as efficient as the corresponding electron trigger, while its weaker isolation requirements yield an event sample that can also be used in sideband analyses to estimate the background to the signal.

The electron candidate must pass the high-energy electron pairs (HEEP) selection, which requires the energy deposition in the ECAL to be consistent with that of an electron. The electron candidates are required to have $p_T > 35\,\text{GeV}$ and $|\eta| < 2.5$. The sum of the energy in the HCAL within a cone defined by $\Delta R = \sqrt{(\Delta\eta)^2 + (\Delta\phi)^2} = 0.15$ (where ϕ is the azimuthal angle) centered around the electron candidate, must be less than 5% of its energy, after it is corrected for jet activity unrelated to the electron. The electron candidate must have a well-matched, prompt track in the $\eta - \phi$ plane that has no more than one hit missing in the inner portion of the tracker. The HEEP selection also requires electrons to be isolated, the requirement for which is that the scalar-p_T sum of tracks within a cone of radius $\Delta R = 0.3$ around the candidate direction, excluding the candidate track, is less than 5 GeV, and the p_T sum of energy depositions in the calorimeters within this cone, taking account of small η-dependent offsets, is less than 3% of the p_T of the candidate.

Muon candidates are required to have $p_T > 53$ GeV and to fall into the acceptance region of $|\eta| < 2.4$. The muon candidate must pass the high-p_T muon identification criteria, which requires that the transverse and longitudinal impact parameters of muon candidates relative to the primary vertex must be < 0.2 cm and < 0.5 cm, respectively. The track of the muon candidate must have at least one hit in the pixel detector and hits in at least six silicon-strip layers, and must contain matched segments in at least two muon detector planes. To suppress backgrounds arising from muons within jets, the scalar-p_T sum of all other tracks in the tracker within a cone of $\Delta R = 0.3$ around the muon candidate track is required to have less than 10% of the p_T of the muon candidate. The relative uncertainty in p_T of the muon track is required to be smaller than 30%.

To reduce loss in signal efficiency from misidentification of the sign of the electron or muon charge at large p_T, the electron and muon are not required to have opposite charges. Since highly energetic muons can produce bremsstrahlung in the ECAL along the direction of the inner-muon trajectory, such muons can be misidentified as electrons. An electron candidate is therefore rejected if there is a muon candidate with p_T greater than 5 GeV whose track is within $\Delta R < 0.1$ relative to the electron candidate track. Only one eμ pair is considered per event. When there is more than one eμ candidate, the pair with the highest invariant mass is selected for the analysis. The statistical interpretation is done based on the shape of the invariant eμ mass distribution of the signal as well as the background.

4.2 Selection in eτ and $\mu\tau$ final states

Events are required to have at least one prompt, isolated light lepton (electron or muon) and one prompt, isolated τ_h. The lepton pair is not required to carry opposite electric charge.

Events that satisfy single-electron or single electromagnetic-cluster triggers are selected for the eτ channel. The electron candidate must pass the HEEP selection, similar to the eμ channel, but with an increased p_T threshold of 50 GeV.

The single muon triggers used in the eμ channel are also used to collect the data samples in the

$\mu\tau$ channel. The muon candidate must pass the high-p_T muon identification criteria, same as in the eμ channel.

The p_T of the leading τ_h should be greater than 50 GeV, and a pseudorapidity cut of $|\eta| < 2.3$ is applied. The τ_h candidates are required to pass anti-jet, anti-electron, and anti-muon discriminants in order to reduce jet $\to \tau_h$, e $\to \tau_h$ and $\mu \to \tau_h$ misidentification probabilities. A convolutional deep neural network is used to construct these discriminants. The neural network combines high level variables including the tau isolation with low level variables such as individual energy deposits in CMS subdetectors, in order to provide the best possible discrimination for τ_h decays against quark and gluon jets, electrons, and muons. Hadronically decaying τ_h leptons in this analysis are required to satisfy the tight working point of the anti-jet discriminator. This working point has an efficiency of about 75% for genuine τ_h, with about 0.4% misidentification rate for quark- and gluon-initiated jets. The τ_h candidates in this analysis are required to pass the loose working point of the anti-electron discriminator, which has an efficiency of about 94% for genuine τ_h events, and a misidentification rate of about 0.5% for electrons. The τ_h candidates are further required to pass the tight working point of the anti-muon discriminator, which has an efficiency of $> 99\%$ for genuine τ_h events, with a misidentification rate of about 0.07% for muons.

It was found that the low transverse mass (m_T) region is dominated by misidentified tau events. So a requirement of $m_T > 120$ GeV is applied, where m_T is defined as:

$$m_T = \sqrt{2p_T^l \cdot p_T^{miss}(1 - \cos\Delta\phi(\vec{p}_T^{\,l}, \vec{p}_T^{\,miss}))}, \quad (1)$$

where l denotes the light lepton, i.e. the electron in the eτ final state and the muon in the $\mu\tau$ final state, respectively, p_T^{miss} is the missing transverse energy vector in the event, and $\Delta\phi$ is the difference in the azimuthal angle between $\vec{p}_T^{\,l}$ and $\vec{p}_T^{\,miss}$.

To remove any overlap with the $\mu\tau$ and eμ final states, a muon veto is applied in the eτ final state, rejecting events if they contain any isolated muon with $p_T > 35$ GeV, $|\eta| < 2.4$, passing high-p_T muon identification criteria, and tracker-based isolation < 0.15. Events with a well-separated electron pair are also rejected. A well-separated electron pair is defined as two electrons, each with $p_T > 10$ GeV, $|\eta| < 2.5$, passing a very loose working point ($> 95\%$ efficiency) of cut-based electron identification criteria, and $\Delta R(e, e) > 0.5$.

In the $\mu\tau$ channel, in order to avoid overlap with the eτ and eμ channels, events are vetoed if they contain a HEEP electron with $p_T > 35$ GeV. Events with a well-separated muon pair are also rejected. A well-separated muon pair is defined as two muons passing the high-p_T identification criteria, with $p_T > 10$ GeV, $|\eta| < 2.4$, tracker-based isolation < 0.15, and with $\Delta R(\mu, \mu) > 0.2$.

If there is more than one eτ or $\mu\tau$ pair in an event, then the pair with highest invariant mass is chosen.

The statistical interpretation is based on the shape of the collinear mass distribution of the signal as well as the background. The collinear mass provides an estimate of the mass of the new resonance or quantum black hole by using their observed decay products. It is reconstructed using the collinear approximation based on the observation that, since the mass scale of the signal is orders of magnitude higher than that of the τ, the τ lepton decay products are highly Lorentz boosted in the direction of the τ candidate. The neutrino momenta can be approximated to have the same direction as the other, visible decay products of the τ, and the component of $\vec{p}_T^{\,miss}$ in the direction of the visible τ lepton decay products is used to estimate

the transverse component of the neutrino momentum. The variable x_τ^{vis}, which is the fraction of energy carried by the visible decay products of the τ, is defined as $x_\tau^{\text{vis}} = p_{\text{T}}^{vis}/(p_T^{vis} + p_{\text{T, coll}}^{miss})$, where $p_{\text{T, coll}}^{miss}$ is the part of the missing transverse energy that is collinear with the p_{T} of the τ_{h}. The collinear mass m_{col} can then be derived from the visible mass m_{vis} of the $e\tau$ or $\mu\tau$ system as $m_{col} = m_{vis}/\sqrt{x_\tau^{vis}}$, where m_{vis} is the invariant mass of the visible decay products.

5 Background estimation

The SM background in the LFV dilepton search includes several processes that produce a final state with two different-flavor charged leptons. For all channels, the dominant background contributions originate from $t\bar{t}$ production. Other less significant backgrounds originate from diboson (WW, WZ, and ZZ) production, $Z \to \ell^+\ell^-$ (ℓ = e, μ, τ), Wγ, and single top quark production processes. All these backgrounds are estimated from MC simulation. Multijet and W+jets processes also contribute due to the misidentification of jets as leptons. These backgrounds are estimated from data.

For the eμ channel, to determine the contributions from W+jets and multijet processes to the $m_{e\mu}$ distribution, a control sample in data is defined using jet-to-electron misidentification rates (F_{e}). The jet-to-electron misidentification rate is measured in data, using a control sample collected with a single electromagnetic-cluster trigger. Data sidebands obtained by either the electron isolation or shower shape variables are used to evaluate the contribution of jets passing the full electron selection in the control sample [41]. The jet-to-electron misidentification rate is then defined as the number of jets passing the full electron selection divided by the number of jet candidates in the sample. The rate is quantified in bins of misidentified electron p_{T} and η. The measured rate is used to estimate the W+jets and multijet contributions using data containing muons that pass the single-muon trigger and the full muon selection, and the number of electron candidates satisfying relaxed selection requirements, but failing the full electron selection. Each event is weighted by the factor $F_{\text{e}}/(1 - F_{\text{e}})$ to determine the overall contribution from the jet backgrounds. To avoid double counting, contributions from events with real leptons are estimated with MC simulations and subtracted from the sample.

Background from jets mimicking muons is estimated in a similar way, where identification criteria are loosened for muons in order to create a control sample enriched with jet candidates that are misidentified as muons. Then jet-to-muon misidentification rate F_μ is defined as the number of jets passing the full muon selection divided by the number of jet candidates in the sample. The rate is quantified in bins of misidentified muon p_{T} and η as well. Events in data that have one well-identified electron and one misidentified muon are selected, with the weight factor $F_\mu/(1 - F_\mu)$ applied to estimate the jet-to-muon misidentification contribution in the signal region. Events with both electron and muon misidentified from jets are not considered since their contribution is expected to be small.

In the $\mu\tau$ and $e\tau$ channels, the most significant background after the $t\bar{t}$ and WW processes comes from W+jets and multijet processes, where jets are misidentified as taus. This background is estimated using collision data, in a control sample with the same selection as the signal region, except for the m_{T} requirement which is inverted to $m_{\text{T}} < 120\,\text{GeV}$. In this low m_{T} control sample, the probability for an accompanying jet to be misidentified as a τ_{h} is computed. Two subsamples are constructed:

- Subsample A contains τ_{h} candidates with a selection similar to the signal region, except the anti-jet discriminator. The τ_{h} candidates in this subsample are required to pass a looser working point of the anti-jet discriminator, and they are required to

fail the tight working point.

- Subsample B contains τ_h with similar requirements as subsample A, but the τ_h candidates in this sample must pass the tight working point of the anti-jet discriminator.

A factor F_τ is calculated from these samples, defined as the ratio of the number of events in subsamples B and A. This factor is calculated as a function of tau candidate p_T, the ratio of tau p_T to the p_T of its parent jet, and the pseudorapidity of the τ_h. The number of events expected from misidentified τ_h in the signal region is estimated from a control sample fulfilling the same criteria as events in the signal region, except that the tau candidates pass the looser working point but fail the tight working point of the anti-jet discriminator. Each event is weighted by the factor F_τ to determine its overall contribution. The contribution of events with real τ_h is estimated with MC simulation and subtracted from the sample.

6 Systematic uncertainties

The uncertainty in the modeling of the invariant or collinear mass distributions reflects the input of three types of systematic effects.

The first type includes those that affect the shape of the mass distributions. For all channels, the dominant uncertainties arise from the leading $t\bar{t}$ and subleading WW backgrounds. They correspond to a 30-50% variation in the number of $t\bar{t}$ and WW events at a dilepton mass scale of 2 TeV. The uncertainy in the WW background is estimated from the envelope of the resummed next-to-next-to-leading-logarithm calculation of the soft-gluon contributions to the cross section at NLO, as presented in Ref. [42], using changes by factors of 2 and 0.5 implemented in the renormalization and factorization scales, respectively. Similarly, uncertainty on $t\bar{t}$ background is estimated by considering the variations in PDF and factorization scales as mentioned in Ref. [43]. Other contributions include the uncertainty in the muon momentum scale, which is around 1–2% for 1 TeV muons and depends on their η and ϕ. The uncertainty in the muon-efficiency scale factor (0.5% for 1 TeV muons) is considered in the $e\mu$ and $\mu\tau$ channels; and the electron-efficiency scale factor is considered in the $e\mu$ and $e\tau$ channels. In the τ channels, the uncertainty on the τ_h identification (5% for 1 TeV taus) and τ_h energy scale (1.5–4% for $p_T(\tau_h) > 100$ GeV, depending on the decay mode) are considered. Uncertainties in the electron p_T scale and resolution, the muon p_T resolution, and the pileup rate are also considered, but they have negligible impact on the total background. The uncertainty in the determination of the trigger efficiency leads to a very small impact on the event yield. The uncertainty associated with the choice of the PDF in the simulation is evaluated according to the PDF4LHC procedure [44].

The energy scale of jets is measured with an uncertainty amounting to a few percent, depending on the jet p_T and η, using the p_T-balance method, which is applied to $Z/\gamma^* \to ee$, $Z/\gamma^* \to \mu\mu$, γ+jets, dijet, and multijet events [45]. The resulting effect on signal and background expectations is evaluated by varying the energies of jets in simulated events within their uncertainties, recalculating all kinematic observables such as $\vec{p}_T^{\,miss}$, and reapplying the event selection criteria. The effect of uncertainties in the energy scale of the unclustered particles and jet energy resolution is evaluated in a similar way. These systematic uncertainties affect the shape of the collinear mass distributions.

Uncertainties of the second type directly influence the normalization of the mass distribution. A systematic uncertainty of 2.5% in the integrated luminosity is taken for the backgrounds and signals. Among the uncertainties in the cross sections used for the normalization of various simulated backgrounds, the 5% uncertainty in the dominant $t\bar{t}$ background is the most

significant. A systematic uncertainty of 50% is applied to the estimate of the misidentified jet background derived from data in all three channels. For tau final states, this uncertainty is obtained by using fake F_τ obtained using an independent control sample of Z ($\to \mu\mu$)+jets events for the estimation of misidentified jet background. It is found that the collinear mass distributions obtained in the signal region using the F_τ calculated from two independent control samples agree within 50% considering the statistical uncertainties especially at high masses ($\geq$ 1.5 TeV). Therefore, an overall 50% systematic uncertainty is assigned to the estimation of this background.

Uncertainties of the third type are associated with limited sizes of event samples in the MC simulation of background processes. In contrast to all other uncertainties, they are not correlated between bins of the invariant mass distribution.

Taking all systematic uncertainties into account, the resulting relative uncertainty in the background shows an increasing trend with mass. This does not significantly affect the sensitivity at large mass values, where the expected number of events from SM processes becomes negligible. All these uncertainties are also considered in the estimation of theoretical signals.

All uncertainties are considered to be correlated across the different data-taking years, with the exception of object-related (leptons, jets, $p_{\mathrm{T}}^{\mathrm{miss}}$) uncertainties, which derive from statistically independent sources, and integrated luminosity uncertainties. No correlation between the different final states is considered, and the analysis results are presented independently for each of the final states.

7 Results

The mass distributions in the eμ, eτ, and $\mu\tau$ channels, shown in Fig. 1, do not show significant deviations from the expected SM background. Upper limits on the product of the production cross section σ and branching fraction B are determined using a Bayesian method with a uniform positive prior probability density for the signal cross section. The nuisance parameters associated with the systematic uncertainties are modeled through log-normal distributions for uncertainties in the normalization. Uncertainties in the shape of the distributions are modeled through "template morphing" techniques. A Markov Chain MC method is used for integration. All limits presented here are at 95% confidence level (CL).

Model-specific limits were obtained for the RPV SUSY, Z$'$, and QBH signals and are shown in Figs. 2, 3, and 4, respectively. A $\widetilde{\nu}_\tau$ in RPV SUSY is excluded up to a mass of 4.2 TeV in the eμ channel, up to 3.7 TeV in the eτ channel, and up to 3.6 TeV for the $\mu\tau$ channel, each for the coupling hypothesis $\lambda = \lambda' = 0.1$. If $\lambda = \lambda' = 0.01$ is assumed, the observed limits drop to 2.2 TeV in the eμ channel, 1.6 TeV in the eτ channel, and 1.6 TeV in the $\mu\tau$ channel. A Z$'$ boson with LFV couplings is excluded up to a mass of 5.0 TeV in the eμ channel, up to 4.3 TeV in the eτ channel, and up to 4.1 TeV in the $\mu\tau$ channel. Quantum black holes derived from an ADD model with $n = 4$ extra dimensions are excluded up to the threshold mass of 5.6 TeV in the eμ channel, 5.2 TeV in the eτ channel, and 5.0 TeV in the $\mu\tau$ channel. The observed and expected lower mass limits obtained in all three channels are summarized in Table 1.

In the narrow-width approximation, the value of σB scales with the RPV couplings, in all three channels. For example in the eμ channel, the following approximation holds [14]:

$$\sigma\mathrm{B} \approx (\lambda'_{311})^2[(\lambda_{132})^2 + (\lambda_{231})^2]/(3(\lambda'_{311})^2 + [(\lambda_{132})^2 + (\lambda_{231})^2]).$$

Using the narrow-width approximation formula of the RPV signal cross section, the cross sec-

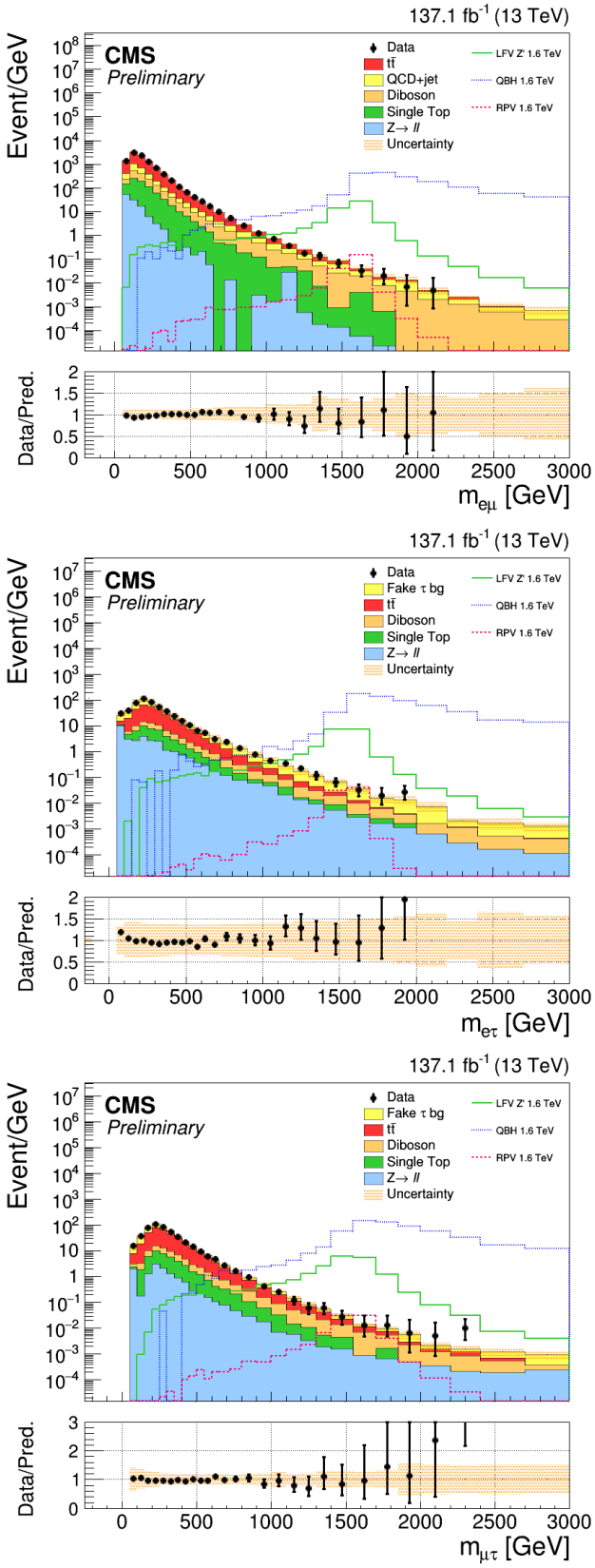

Figure 1: Invariant mass distributions for the eμ channel (top), and collinear mass distributions for the eτ (middle) and $\mu\tau$ (bottom) channels. In addition to the observed data (black points) and standard model expectation (filled histograms), expected signal distributions for three models are shown: the RPV SUSY model with $\lambda = \lambda' = 0.01$ and sneutrino mass of 1.6 TeV, a Z′ boson with a mass of 1.6 TeV, and the QBH expectation for $n = 4$ and a threshold mass of 1.6 TeV.

Channel	RPV (TeV)		Z′ (TeV)	QBH (TeV)
	$\lambda = \lambda' = 0.01$	$\lambda = \lambda' = 0.1$		
eμ	2.2 (2.2)	4.2 (4.2)	5.0 (4.9)	5.6 (5.6)
eτ	1.6 (1.6)	3.7 (3.7)	4.3 (4.3)	5.2 (5.2)
$\mu\tau$	1.6 (1.6)	3.6 (3.7)	4.1 (4.2)	5.0 (5.0)

Table 1: The observed and expected (in brackets) 95% CL lower mass limits on RPV SUSY, Z′, and QBH signals for the eμ, eτ, and $\mu\tau$ channels.

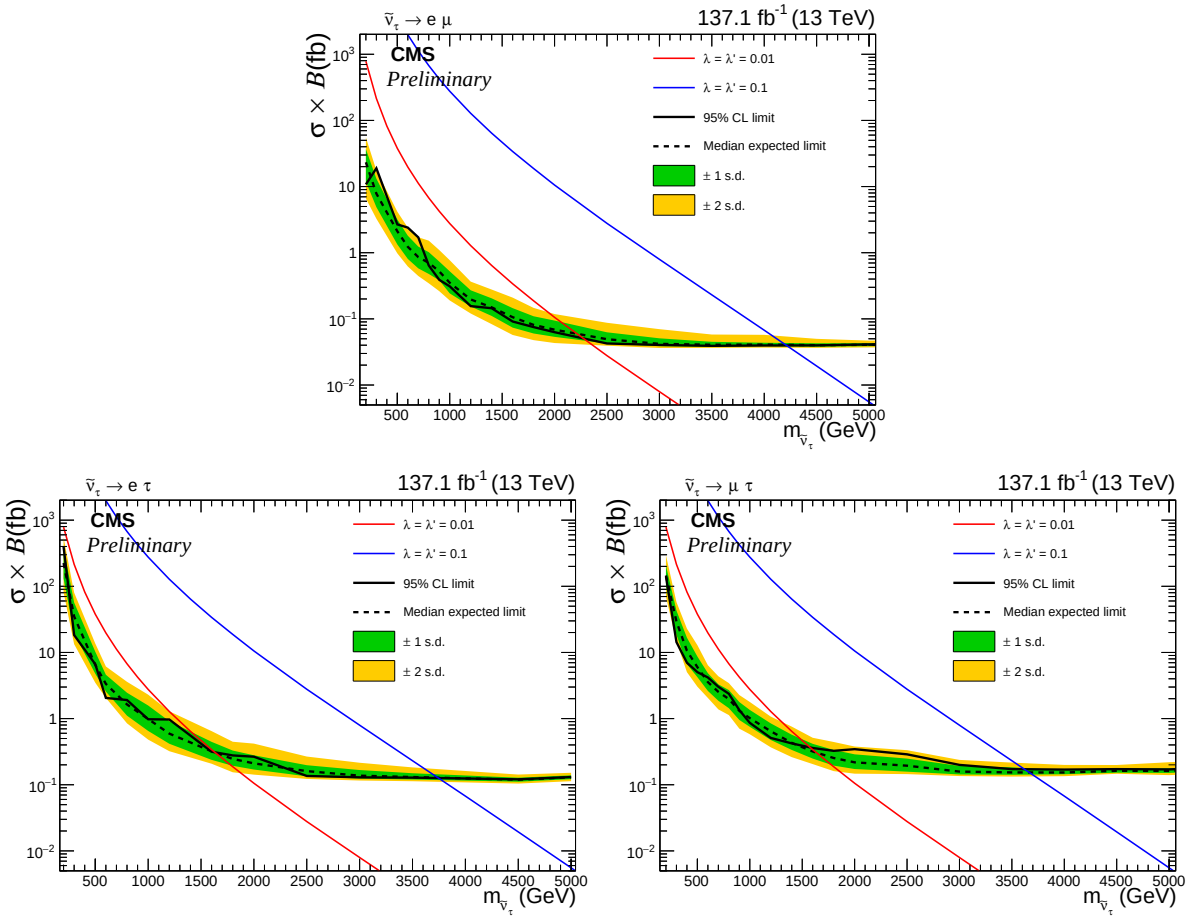

Figure 2: Expected (black dashed line) and observed (black solid line) 95% CL upper limits on the product of cross section times branching fraction as a function of the tau sneutrino mass in an RPV SUSY model for the eμ (top), eτ (bottom left), and $\mu\tau$ (bottom right) channels. The shaded bands represent the one and two standard deviation (s.d.) uncertainties.

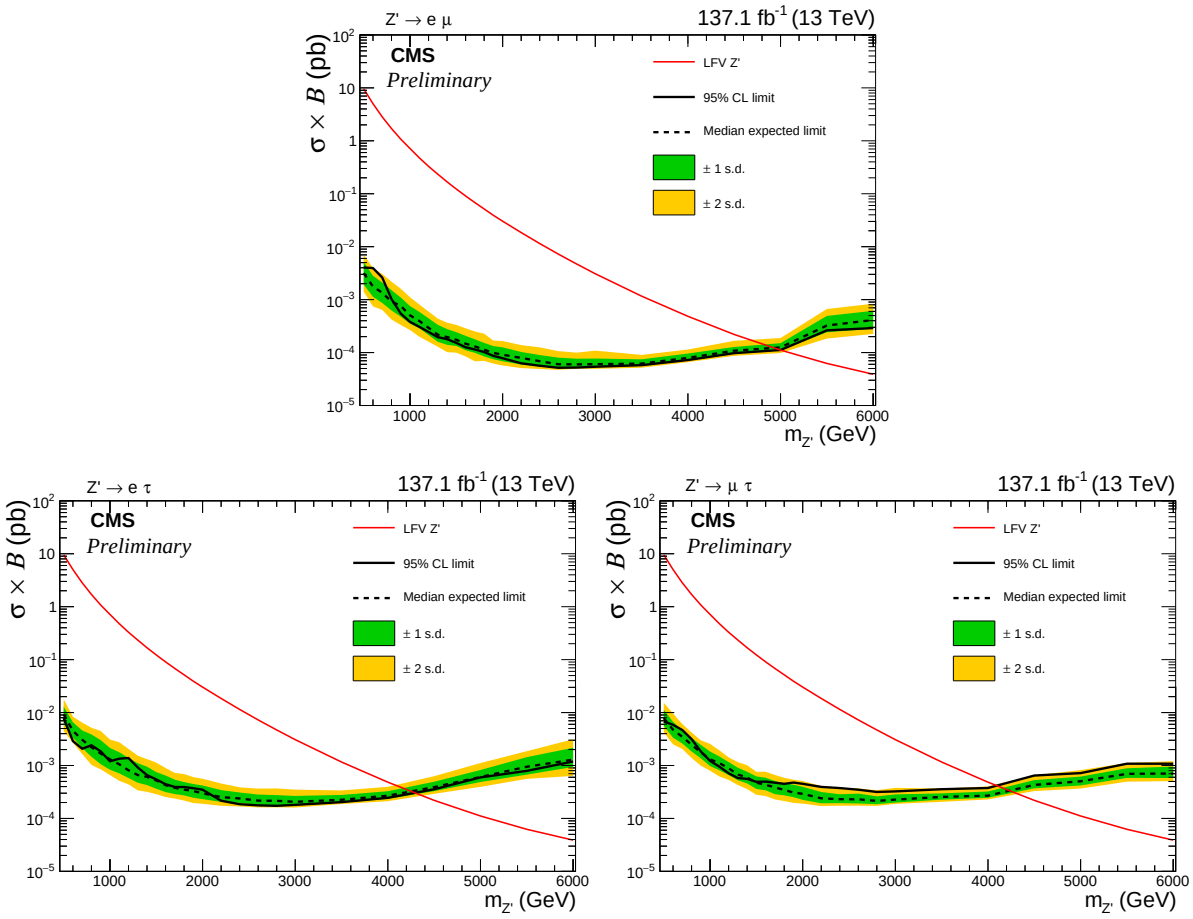

Figure 3: Expected (black dashed line) and observed (black solid line) 95% CL upper limits on the product of cross section and branching fraction for a Z′ boson with LFV decays, in the eμ (top), eτ (bottom left), and $\mu\tau$ (bottom right) channels. The shaded bands represent the one and two standard deviation (s.d.) uncertainties.

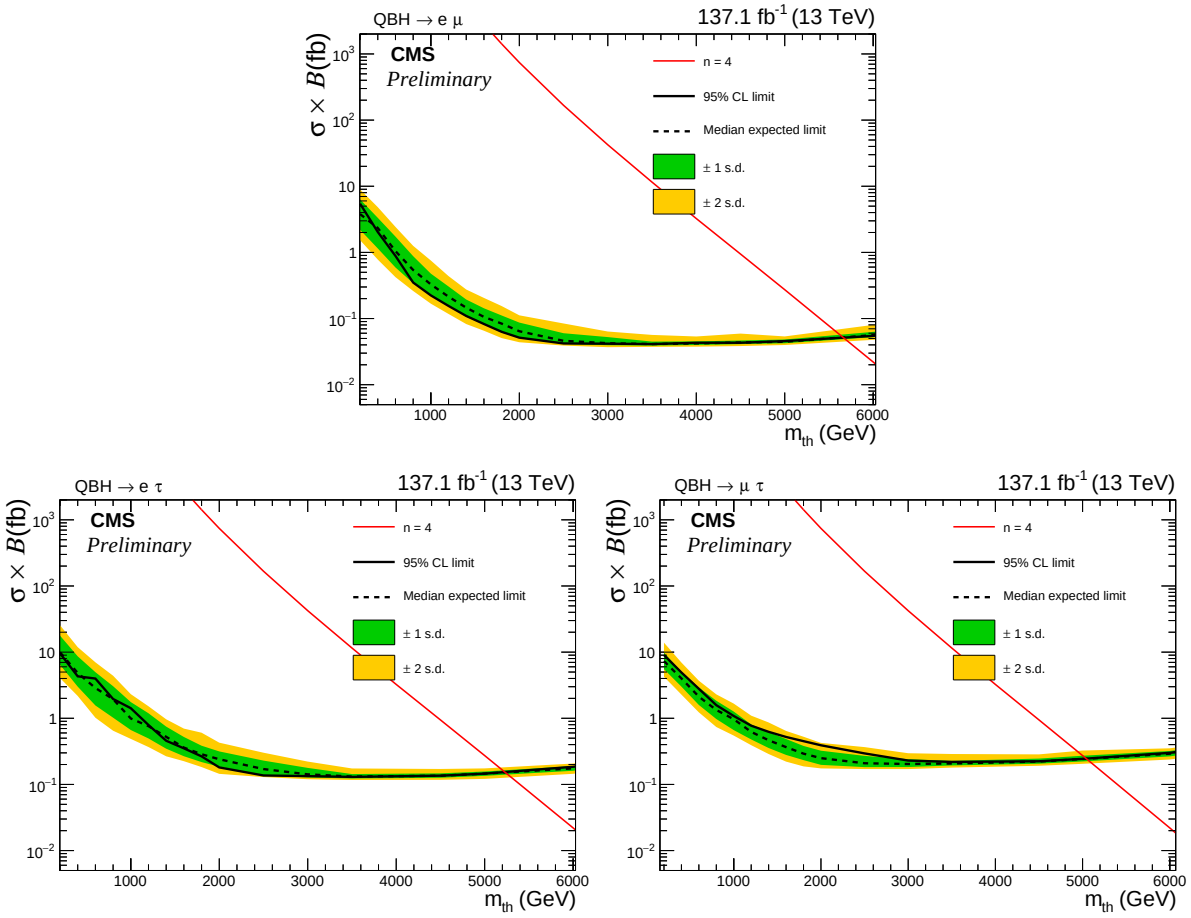

Figure 4: Expected (black dashed line) and observed (black solid line) 95% CL upper limits on the product of cross section and branching fraction for quantum black hole production in an ADD model with $n = 4$ extra dimensions, in the eμ (top), eτ (bottom left), and $\mu\tau$ (bottom right) channels. The shaded bands represent the one and two standard deviation (s.d.) uncertainties.

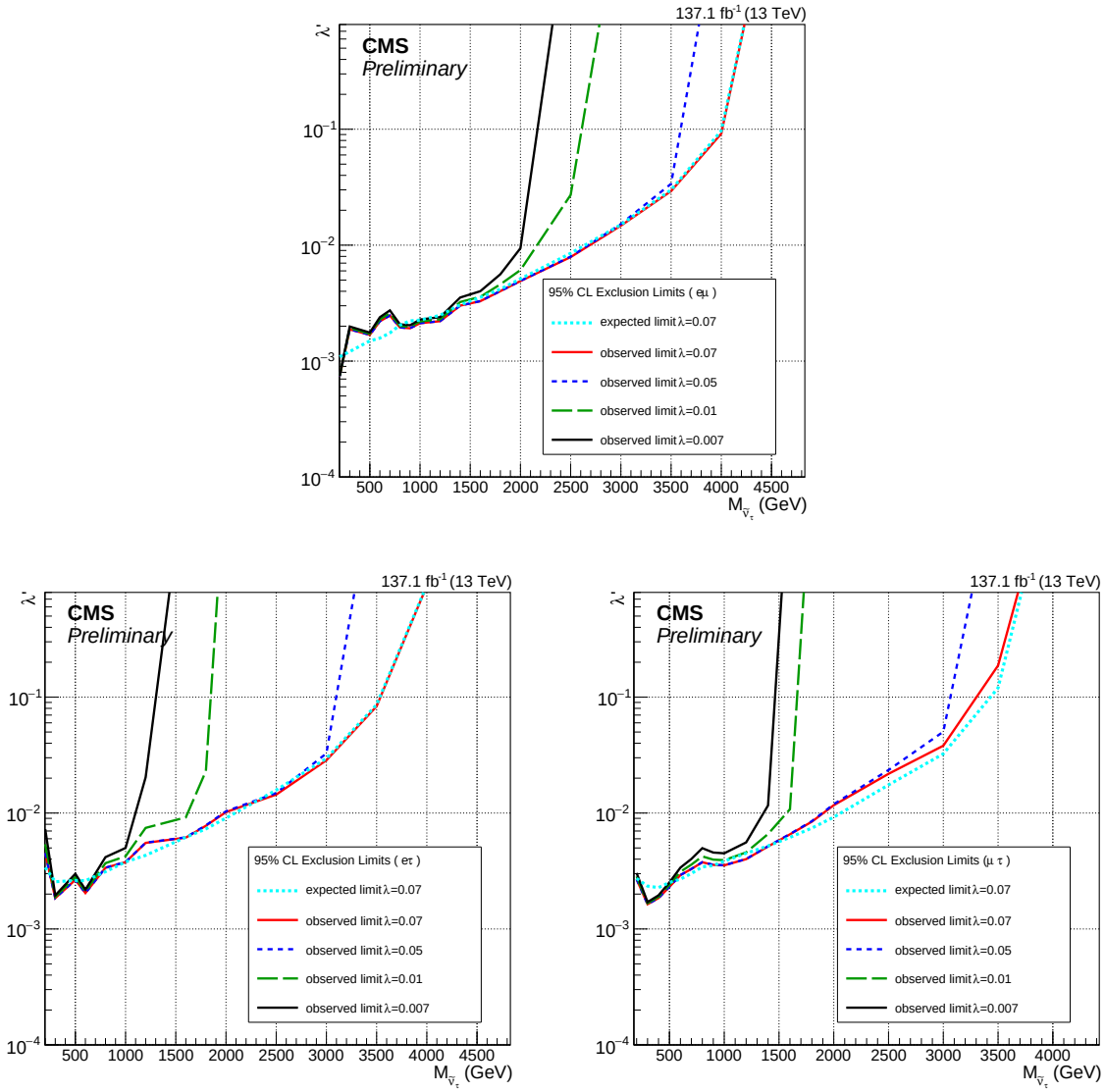

Figure 5: Upper limits at 95% CL on the RPV SUSY model in the plane of sneutrino mass and λ' coupling, for four values of λ couplings. The regions to the left of and above the limits are excluded. The top plot corresponds to the eμ channel, while the bottom left and right plot show the eτ and $\mu\tau$ channels, respectively.

tion limit is translated into exclusion bounds in the plane of mass and coupling of the parameter space of the RPV SUSY model for fixed values of the λ couplings responsible for the decay of the tau sneutrino. Limit contours in the plane of mass and coupling for several fixed values of the coupling are shown in Fig 5.

Model-independent cross section limits are also obtained. The model-specific shape analysis assumes a certain signal shape in invariant (eμ channel) or collinear mass (τ channels). However, alternative new physics processes yielding lepton flavor violating final states could cause an excess of a different shape. A model-independent cross section limit is determined using a single bin ranging from a lower threshold on invariant (collinear) mass to infinity. No assumptions on the shape of the signal distribution are made other than that of a flat product of acceptance times efficiency, Aϵ, as a function of the mass. In order to determine the limit for a specific model from the model-independent limit shown here, the model-dependent part of the efficiency needs to be applied. The experimental efficiencies for the signal are already taken into account.

A factor f_m that reflects the effect of the threshold $m^{\min}$ on the signal is determined by counting the events with $m > m^{\min}$ and dividing the result by the number of MC generated events. The reconstruction efficiency is nearly constant over the entire mass range probed here, therefore f_m can be evaluated at generator level. A limit on the product of the cross section and branching fraction $(\sigma \mathrm{BA}\epsilon)_{\mathrm{excl}}$ can be obtained by dividing the excluded cross section of the model-independent limit $(\sigma \mathrm{BA}\epsilon)_{\mathrm{MI}}$ given in Fig. 6 by the calculated fraction $f_m(m^{\min})$:

$$(\sigma \mathrm{BA}\epsilon)_{\mathrm{excl}} = \frac{(\sigma BA\epsilon)_{MI} m^{\min}}{f_m(m^{\min})}. \tag{2}$$

Here, B is the branching fraction of the new particle decaying to a lepton flavor violating final state. Models with a theoretical cross section $(\sigma \mathrm{B})_{\mathrm{theo}}$ larger than $(\sigma \mathrm{B})_{\mathrm{excl}}$ can be excluded. The procedure described here can be applied to all models involving the two-body decay of a massive state, which exhibit back-to-back kinematics similar to those of a generic Z'. The fraction of events $f_m(m^{\min})$ must be determined for the particular model under consideration.

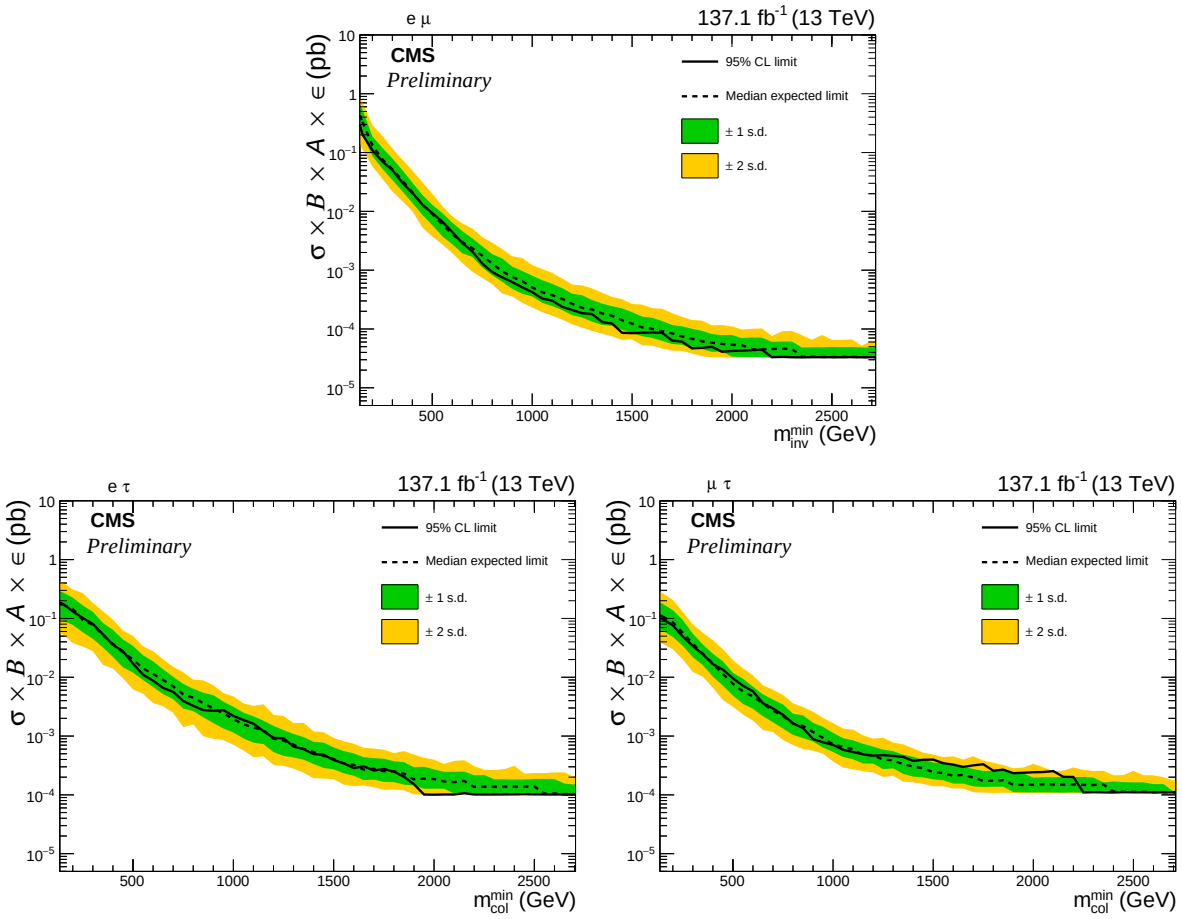

Figure 6: Model independent upper limits at 95% CL on the product of cross section, branching fraction, acceptance, and efficiency are shown. Observed (expected) limits are shown in black solid (dashed) lines for the eμ (top), eτ (bottom left), and $\mu\tau$ (bottom right) channels. The shaded bands represent the one and two standard deviation (s.d.) uncertainties.

8 Summary

A search for heavy particles decaying into $e\mu$, $e\tau$, or $\mu\tau$ final states is conducted using 137.1 fb^{-1} of proton-proton collision data at $\sqrt{s} = 13$ TeV recorded by the CMS detector at the LHC. The data are consistent with the standard model predictions, and lower limits at 95% confidence level are set on the mass of a supersymmetric τ sneutrino with R-parity-violating couplings $\lambda = \lambda' = 0.1$ at 4.2 ($e\mu$ channel), 3.7 ($e\tau$), and 3.6 TeV ($\mu\tau$), respectively; on the mass of a Z' vector boson with lepton-flavor violating couplings at 5.0 ($e\mu$), 4.3 ($e\tau$), and 4.1 TeV ($\mu\tau$), respectively; and on the threshold mass for quantum black hole production in the context of the Arkani-Hamed-Dimopoulos-Dvali model with four extra dimensions at 5.6 ($e\mu$), 5.2 ($e\tau$), and 5.0 TeV ($\mu\tau$). In addition, model-independent limits are provided allowing the results to be interpreted in other models with the same final states and similar kinematic distributions. Limits in the $e\tau$ and $\mu\tau$ final states as well as model-independent limits are reported by CMS for the first time, and all results of this search are currently the best limits from the LHC in the considered models.

References

[1] G. R. Farrar and P. Fayet, "Phenomenology of the production, decay, and detection of new hadronic states associated with supersymmetry", *Phys. Lett. B* **76** (1978) 575, doi:10.1016/0370-2693(78)90858-4.

[2] F. de Campos et al., "CERN LHC signals for neutrino mass model in bilinear R-parity violating mAMSB", *Phys. Rev. D* **77** (2008) 115025, doi:10.1103/PhysRevD.77.115025, arXiv:0803.4405.

[3] R. Barbier et al., "R-parity violating supersymmetry", *Phys. Rept.* **420** (2005) 1, doi:10.1016/j.physrep.2005.08.006, arXiv:hep-ph/0406039.

[4] P. Langacker, "The physics of heavy Z' gauge bosons", *Rev. Mod. Phys.* **81** (2009) 1199, doi:10.1103/RevModPhys.81.1199, arXiv:0801.1345.

[5] X. Calmet, W. Gong, and S. D. H. Hsu, "Colorful quantum black holes at the LHC", *Phys. Lett. B* **668** (2008) 20, doi:10.1016/j.physletb.2008.08.011, arXiv:0806.4605.

[6] P. Meade and L. Randall, "Black holes and quantum gravity at the LHC", *JHEP* **05** (2008) 003, doi:10.1088/1126-6708/2008/05/003, arXiv:0708.3017.

[7] P. W. Graham, D. E. Kaplan, S. Rajendran, and P. Saraswat, "Displaced supersymmetry", *JHEP* **07** (2012) 149, doi:10.1007/JHEP07(2012)149, arXiv:1204.6038.

[8] D. M. Gingrich, "Quantum black holes with charge, colour, and spin at the LHC", *J. Phys. G* **37** (2010) 105008, doi:10.1088/0954-3899/37/10/105008, arXiv:0912.0826.

[9] L. Randall and R. Sundrum, "A large mass hierarchy from a small extra dimension", *Phys. Rev. Lett.* **83** (1999) 3370, doi:10.1103/PhysRevLett.83.3370, arXiv:hep-ph/9905221.

[10] N. Arkani-Hamed, S. Dimopoulos, and G. R. Dvali, "The hierarchy problem and new dimensions at a millimeter", *Phys. Lett. B* **429** (1998) 263, doi:10.1016/S0370-2693(98)00466-3, arXiv:hep-ph/9803315.

[11] CDF Collaboration, "Search for R-parity violating decays of τ sneutrinos to eμ, $\mu\tau$, and eτ pairs in $p\bar{p}$ collisions at $\sqrt{s} = 1.96$ TeV", *Phys. Rev. Lett.* **105** (2010) 191801, doi:10.1103/PhysRevLett.105.191801, arXiv:1004.3042.

[12] D0 Collaboration, "Search for sneutrino production in eμ final states in 5.3 fb^{-1} of $p\bar{p}$ collisions at $\sqrt{s} = 1.96$ TeV", *Phys. Rev. Lett.* **105** (2010) 191802, doi:10.1103/PhysRevLett.105.191802, arXiv:1007.4835.

[13] ATLAS Collaboration, "Search for a heavy neutral particle decaying to eμ, eτ, or $\mu\tau$ in pp collisions at $\sqrt{s} = 8$ TeV with the ATLAS detector", *Phys. Rev. Lett.* **115** (2015) 031801, doi:10.1103/PhysRevLett.115.031801, arXiv:1503.04430.

[14] CMS Collaboration, "Search for lepton flavour violating decays of heavy resonances and quantum black holes to an eμ pair in proton-proton collisions at $\sqrt{s}$ = 8 TeV", *Eur. Phys. J. C* **76** (2016) 317, doi:10.1140/epjc/s10052-016-4149-y, arXiv:1604.05239.

[15] ATLAS Collaboration, "Search for new phenomena in different-flavour high-mass dilepton final states in pp collisions at $\sqrt{s} = 13$ TeV with the ATLAS detector", *Eur. Phys. J. C* **76** (2016) 541, doi:10.1140/epjc/s10052-016-4385-1, arXiv:1607.08079.

[16] CMS Collaboration, "Search for lepton-flavor violating decays of heavy resonances and quantum black holes to eμ final states in proton-proton collisions at $\sqrt{s} = 13$ TeV", *JHEP* **04** (2018) 073, doi:10.1007/JHEP04(2018)073, arXiv:1802.01122.

[17] ATLAS Collaboration, "Search for lepton-flavor violation in different-flavor, high-mass final states in pp collisions at $\sqrt{s} = 13$ TeV with the ATLAS detector", *Phys. Rev. D* **98** (2018) 092008, doi:10.1103/PhysRevD.98.092008, arXiv:1807.06573.

[18] CMS Collaboration, "Description and performance of track and primary-vertex reconstruction with the CMS tracker", *JINST* **9** (2014) P10009, doi:10.1088/1748-0221/9/10/P10009, arXiv:1405.6569.

[19] CMS Collaboration, "Performance of electron reconstruction and selection with the CMS detector in proton-proton collisions at $\sqrt{s} = 8$ TeV", *JINST* **10** (2015) P06005, doi:10.1088/1748-0221/10/06/P06005, arXiv:1502.02701.

[20] CMS Collaboration, "Performance of the CMS muon detector and muon reconstruction with proton-proton collisions at $\sqrt{s} = 13$ TeV", *JINST* **13** (2018) P06015, doi:10.1088/1748-0221/13/06/P06015, arXiv:1804.04528.

[21] CMS Collaboration, "The CMS experiment at the CERN LHC", *JINST* **3** (2008) S08004, doi:10.1088/1748-0221/3/08/S08004.

[22] A. Belyaev, N. D. Christensen, and A. Pukhov, "CalcHEP 3.4 for collider physics within and beyond the standard model", *Comput. Phys. Commun.* **184** (2013) 1729, doi:10.1016/j.cpc.2013.01.014, arXiv:1207.6082.

[23] T. Sjöstrand, S. Mrenna, and P. Z. Skands, "A brief introduction to PYTHIA 8.1", *Comput. Phys. Commun.* **178** (2008) 852, doi:10.1016/j.cpc.2008.01.036, arXiv:0710.3820.

[24] J. Pumplin et al., "New generation of parton distributions with uncertainties from global QCD analysis", *JHEP* **07** (2002) 012, doi:10.1088/1126-6708/2002/07/012, arXiv:hep-ph/0201195.

[25] NNPDF Collaboration, "Parton distributions for the LHC run II", *JHEP* **04** (2015) 040, doi:10.1007/JHEP04(2015)040, arXiv:1410.8849.

[26] J. Alwall et al., "The automated computation of tree-level and next-to-leading order differential cross sections, and their matching to parton shower simulations", *JHEP* **07** (2014) 079, doi:10.1007/JHEP07(2014)079, arXiv:1405.0301.

[27] R. Frederix and S. Frixione, "Merging meets matching in MC@NLO", *JHEP* **12** (2012) 061, doi:10.1007/JHEP12(2012)061, arXiv:1209.6215.

[28] P. Nason, "A new method for combining NLO QCD with shower Monte Carlo algorithms", *JHEP* **11** (2004) 040, doi:10.1088/1126-6708/2004/11/040, arXiv:hep-ph/0409146.

[29] S. Frixione, P. Nason, and C. Oleari, "Matching NLO QCD computations with parton shower simulations: the POWHEG method", *JHEP* **11** (2007) 070, doi:10.1088/1126-6708/2007/11/070, arXiv:0709.2092.

[30] S. Alioli, P. Nason, C. Oleari, and E. Re, "A general framework for implementing NLO calculations in shower Monte Carlo programs: the POWHEG BOX", *JHEP* **06** (2010) 043, doi:10.1007/JHEP06(2010)043, arXiv:1002.2581.

[31] S. Frixione, P. Nason, and G. Ridolfi, "A positive-weight next-to-leading-order Monte Carlo for heavy flavour hadroproduction", *JHEP* **09** (2007) 126, doi:10.1088/1126-6708/2007/09/126, arXiv:0707.3088.

[32] CMS Collaboration, "Event generator tunes obtained from underlying event and multiparton scattering measurements", *Eur. Phys. J. C* **76** (2016) 155, doi:10.1140/epjc/s10052-016-3988-x, arXiv:1512.00815.

[33] GEANT4 Collaboration, "GEANT4—a simulation toolkit", *Nucl. Instrum. Meth. A* **506** (2003) 250, doi:10.1016/S0168-9002(03)01368-8.

[34] J. Allison et al., "GEANT4 developments and applications", *IEEE Trans. Nucl. Sci.* **53** (2006) 270, doi:10.1109/TNS.2006.869826.

[35] J. Allison et al., "Recent developments in GEANT4", *Nucl. Instrum. Meth. A* **835** (2016) 186, doi:10.1016/j.nima.2016.06.125.

[36] CMS Collaboration, "Particle-flow reconstruction and global event description with the CMS detector", *JINST* **12** (2017) P10003, doi:10.1088/1748-0221/12/10/P10003, arXiv:1706.04965.

[37] M. Cacciari, G. P. Salam, and G. Soyez, "The anti-k_t jet clustering algorithm", *JHEP* **04** (2008) 063, doi:10.1088/1126-6708/2008/04/063, arXiv:0802.1189.

[38] M. Cacciari, G. P. Salam, and G. Soyez, "Fastjet user manual", *Eur. Phys. J. C* **72** (2012) 1896, doi:10.1140/epjc/s10052-012-1896-2, arXiv:1111.6097.

[39] CMS Collaboration, "Performance of reconstruction and identification of τ leptons decaying to hadrons and ν_τ in pp collisions at $\sqrt{s} = 13$ TeV", *JINST* **13** (2018) P10005, doi:10.1088/1748-0221/13/10/P10005, arXiv:1809.02816.

[40] CMS Collaboration, "Performance of the DeepTau algorithm for the discrimination of taus against jets, electron, and muons", CMS Detector Performance Summary CMS-DP-2019-033, 2019.

[41] CMS Collaboration, "Search for resonant and nonresonant new phenomena in high-mass dilepton final states at $\sqrt{s} = 13$ TeV", *JHEP* **07** (2021) 208, doi:10.1007/JHEP07(2021)208, arXiv:2103.02708.

[42] B. D. Pecjak, D. J. Scott, X. Wang, and L. L. Yang, "Resummed differential cross sections for top-quark pairs at the LHC", *Phys. Rev. Lett.* **116** (2016) 202001, doi:10.1103/PhysRevLett.116.202001, arXiv:1601.07020.

[43] M. Czakon et al., "Top-pair production at the LHC through NNLO QCD and NLO EW", *JHEP* **10** (2017) 186, doi:10.1007/JHEP10(2017)186, arXiv:1705.04105.

[44] J. Butterworth et al., "PDF4LHC recommendations for LHC Run II", *J. Phys. G* **43** (2016) 023001, doi:10.1088/0954-3899/43/2/023001, arXiv:1510.03865.

[45] CMS Collaboration, "Jet energy scale and resolution in the CMS experiment in pp collisions at 8 TeV", *JINST* **12** (2017) P02014, doi:10.1088/1748-0221/12/02/P02014, arXiv:1607.03663.